Electronic Supporting Information (ESI)

Crystallographic Characterization of $Er_3N@C_{2n}$ (2n = 80, 82, 84, 88): The Importance of a Planar Er_3N Cluster

Shuaifeng Hu[a] *Pei Zhao,*[b] *Wangqiang Shen,*[a] *Pengyuan Yu,*[a] *Wenhuan Huang**[c] *Masahiro Ehara,**[b] *Yunpeng Xie,**[a] *Takeshi Akasaka,**[a] *and Xing Lu**[a]

[a]State Key Laboratory of Materials Processing and Die & Mould Technology, School of Materials Science and Engineering, Huazhong University of Science and Technology, 1037 Luoyu Road, Wuhan, 430074, China. E-mail: lux@hust.edu.cn.

[b]Research Center for Computational Science, Institute for Molecular Science, Okazaki, 444-8585, Japan. E-mail: ehara@ims.ac.jp.

[c]Shaanxi Key Laboratory of Chemical Additives for Industry, College of Chemistry & Chemical Engineering, Shaanxi University of Science & Technology, Xi'an 710021, China. E-mail: huangwenhuan@sust.edu.cn.

Table of Contents

Experimental section

High-performance liquid chromatography (HPLC) separation processes of $Er_3N@C_{80\text{-}88}$.

Fig. S1 Isolation scheme of the fullerene extract.

Fig. S2 Isolation schemes of $Er_3N@I_h(7)\text{-}C_{80}$ and $Er_3N@D_{5h}(6)\text{-}C_{80}$.

Fig. S3 Isolation schemes of $Er_3N@C_{2v}(9)\text{-}C_{82}$.

Fig. S4 Isolation schemes of Fr8.

Fig. S5 Isolation schemes of $Er_3N@C_s(51365)\text{-}C_{84}$.

Fig. S6 Isolation schemes of $Er_3N@D_3(17)\text{-}C_{86}$ and $Er_3N@D_2(35)\text{-}C_{88}$.

Table S1. The details of the vis-NIR absorptions of $Er_3N@C_{80\text{-}88}$ isomers.

Table S2. Crystallographic data of $Er_3N@I_h(7)\text{-}C_{80}/Ni^{II}(OEP)$, $Er_3N@D_{5h}(6)\text{-}C_{80}/Ni^{II}(OEP)$, $Er_3N@C_{2v}(9)\text{-}C_{82}/Ni^{II}(OEP)$, $Er_3N@C_s(51365)\text{-}C_{84}/Ni^{II}(OEP)$, and $Er_3N@D_2(35)\text{-}C_{88}/1.5Ni^{II}(OEP)$.

Table S3. The fractional occupancies of the Er positions in $Er_3N@I_h(7)\text{-}C_{80}$, $Er_3N@D_{5h}(6)\text{-}C_{80}$, $Er_3N@C_{2v}(9)\text{-}C_{82}$, $Er_3N@C_s(51365)\text{-}C_{84}$, and $Er_3N@D_2(35)\text{-}C_{88}$.

Fig. S7 Packing structures of $Er_3N@I_h(7)\text{-}C_{80}\cdot Ni^{II}(OEP)$, $Er_3N@D_{5h}(6)\text{-}C_{80}\cdot Ni^{II}(OEP)$, $Er_3N@C_{2v}(9)\text{-}C_{82}\cdot Ni^{II}(OEP)$, $Er_3N@C_s(51365)\text{-}C_{84}\cdot Ni^{II}(OEP)$, and $Er_3N@D_2(35)\text{-}C_{88}\cdot 1.5Ni^{II}(OEP)$.

Fig. S8 The Er-N distances of the major Er_3N site as a function of the cage size.

Fig. S9 Optimized molecular structure of $Er_3N@D_3(17)\text{-}C_{86}$.

Table S4. Values of the main molecular orbitals for $Er_3N@C_{80\text{-}88}$.

Fig. S10 Main molecular orbitals of $Er_3N@C_{80\text{-}88}$.

References

Experimental section:

General Characterization. HPLC was conducted on an LC-908 machine (Japan Analytical Industry Co., Ltd.) with toluene/chlorobenzene as mobile phase. LDI-TOF mass spectrometry was measured on a BIFLEX III spectrometer (Bruker Daltonics Inc., Germany). Vis-NIR spectra were obtained from a PE Lambda 750S spectrophotometer in carbon disulfide. CV results were obtained in o-dichlorobenzene using a CHI-660E instrument. A conventional three-electrode cell consisting of a platinum counter electrode, a glassy carbon working electrode, and a silver reference electrode was used for all measurements. $TBAPF_6$ (0.05 M) was used as the supporting electrolyte and ferrocene was added as an internal reference at the end of the experiments for measuring the potentials. The CVs were measured at a scan rate of 100 mV s^{-1} at room temperature under nitrogen protection.

Preparation and Isolation of $Er_3N@C_{2n}$ ($2n$ = 80-88). Graphite rods were core-drilled and subsequently packed with a mixture of Er_2O_3 and graphite powder with a molar ratio of 1:30. Then, the packed rods were preheated at about 1000 °C under Ar flow for about 10 h to remove air and moisture. These rods were then vaporized in a Krätschmer-Huffman generator under a mixture of 220 Torr helium and 30 Torr dinitrogen gases with a power of 110 A × 30 V. Then, the soot was collected and sonicated in carbon disulfide for 1 h under argon atmosphere.

After solvent removal, the extracted fullerenes were dissolved in toluene and the solution was subjected to HPLC separations. (See below)

Single crystal XRD measurements of $Er_3N@I_h(7)-C_{80}$, $Er_3N@D_{5h}(6)-C_{80}$, $Er_3N@C_{2v}(9)-C_{82}$, $Er_3N@C_s(51365)-C_{84}$, and $Er_3N@D_2(35)-C_{88}$. Crystalline blocks of $Er_3N@C_{2n}$ ($2n$ = 80, 82, 84, 88) isomers were obtained by layering a benzene solution of Ni^{II}(OEP) over a carbon disulfide solution of EMFs at 0 ºC. Over a 20-day period, the two solutions diffused together, and black crystals formed. Single-crystal XRD measurements of $Er_3N@I_h(7)-C_{80}$, $Er_3N@D_{5h}(6)-C_{80}$, and $Er_3N@C_{2v}(9)-C_{82}$, were performed at 173 K on a Bruker D8 QUEST machine equipped with a CMOS camera (Bruker AXS Inc., Germany). Crystallographic characterization of $Er_3N@C_s(51365)-C_{84}$, and $Er_3N@D_2(35)-C_{88}$ were performed at 100 K using synchrotron radiation with a MarCCD detector at beamline BL17B station of Shanghai Synchrotron Radiation Facility.[1] The multiscan method was used for absorption corrections. The structures were solved by direct method and were refined with SHELXL-2018/1.[2] CCDC-1915695 ($Er_3N@I_h(7)-C_{80}$), CCDC-1915696 ($Er_3N@D_{5h}(6)-C_{80}$), CCDC-1915697 ($Er_3N@C_{2v}(9)-C_{82}$), CCDC-1915698 ($Er_3N@C_s(51365)-C_{84}$), and CCDC-1915699 ($Er_3N@D_2(35)-C_{88}$) contain the supplementary crystallographic data for this paper.

Computational details. All $Er_3N@C_{2n}$ isomers were optimized using the UB3LYP[3-5] functional with the basis sets of 3-21G (for C and N) and SDD~ECP28MWB_SEG[6, 7] (for Er). The calculations were performed at the tenfold spin state due to the formal valence electronic configuration of erbium ($4f^{11}$). All DFT calculations were carried out using the Gaussian 09 program package.[8]

High-performance liquid chromatography (HPLC) separation processes of $Er_3N@C_{80-88}$.

The first stage was performed on a 5PYE column (20 mm × 250 mm, Cosmosil Nacalai Tesque) with toluene as mobile phase. Fig. S1 shows the corresponding chromatogram. Three fractions, which are named as Fr5, Fr7, and Fr8 were collected. Then, Fr5 was injected into a Buckyprep-M column (20 mm × 250 mm, Cosmosil Nacalai Tesque) for the second stage separation using toluene as eluent, and Fr5-2 was obtained (Fig. S2a). Fr5-2 was then injected into a 5PBB column (20 mm × 250 mm, Cosmosil Nacalai Tesque) for the third stage separation using chlorobenzene as the eluent, and pure $Er_3N@C_{80}$ (I) and $Er_3N@C_{80}$ (II) were finally obtained (Fig. S2b).

As for Fr7, a Buckyprep-M column (20 mm × 250 mm, Cosmosil Nacalai Tesque) was used for the second stage separation, and then fraction Fr7-2 was collected (Fig. S3a). In the third stage, Fr7-2 was injected into a 5PYE column (20 mm × 250 mm, Cosmosil Nacalai Tesque), and then fraction Fr7-2-3 was collected (Fig. S3b). After that, Fr7-2-3 was injected into a Buckyprep column (20 mm × 250 mm, Cosmosil Nacalai Tesque) for the final separation, and pure $Er_3N@C_{2v}(9)\text{-}C_{82}$ was obtained (Fig. S3c). Toluene was used as eluent in all separations here.

In the second stage for the purification of $Er_3N@C_s(51365)\text{-}C_{84}$, $Er_3N@D_3(17)\text{-}C_{86}$ and $Er_3N@D_2(35)\text{-}C_{88}$, a 5PBB column (20 mm × 250 mm, Cosmosil Nacalai Tesque) was used to separate Fr8 with chlorobenzene flow, then Fr8-2 and Fr8-4 were collected (Fig. S4). In the third stage separation, Fr8-2 and Fr8-4 were injected into a Buckyprep-M column (20 mm × 250 mm, Cosmosil Nacalai Tesque), respectively, using chlorobenzene as eluent, and Fr8-2-2 and Fr8-4-2 were collected, respectively (Fig. S5a and Fig. S6a). In the fourth stage, Fr8-2-2 and Fr8-4-2 were injected into a Buckyprep column (20 mm × 250 mm, Cosmosil Nacalai Tesque), respectively, using chlorobenzene as eluent, and Fr8-2-2-1 and Fr8-4-2-1 were collected, respectively (Fig. S5b and Fig. S6b). Then, for pure $Er_3N@C_s(51365)\text{-}C_{84}$ obtain, two steps on a Buckyprep column (20 mm × 250 mm, Cosmosil Nacalai Tesque) was used for Fr8-2-2-1separation with toluene as mobile phase (Fig. S5c and Fig. S5d). For Fr8-4-2-1, a 5PBB column (10 mm × 250 mm, Cosmosil Nacalai Tesque) was used for the following separation with chlorobenzene as mobile phase, and Fr8-4-2-1-1 and Fr8-4-2-1-2 were collected, respectively. At last, Fr8-4-2-1-1 was injected into a Buckyprep column (10 mm × 250 mm, Cosmosil Nacalai Tesque) with toluene flow, and pure $Er_3N@D_3(17)\text{-}C_{86}$ was obtained (Fig. S6d). Meanwhile, for the pure $Er_3N@D_2(35)\text{-}C_{88}$ collection, Fr8-4-2-1-2 was injected into a Buckyprep column (20 mm × 250 mm, Cosmosil Nacalai Tesque) with toluene as mobile phase for the final separation (Fig. S6e).

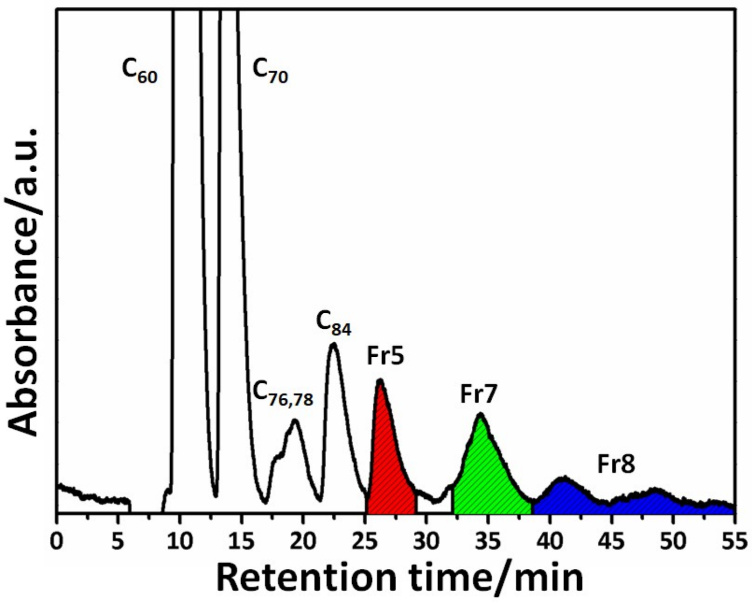

Fig. S1 Isolation scheme of the fullerene extract on a 5PYE column. Conditions: eluent: toluene, 10 mL/min flow rate; inject volume: 15 mL; 330 nm detecting wavelength.

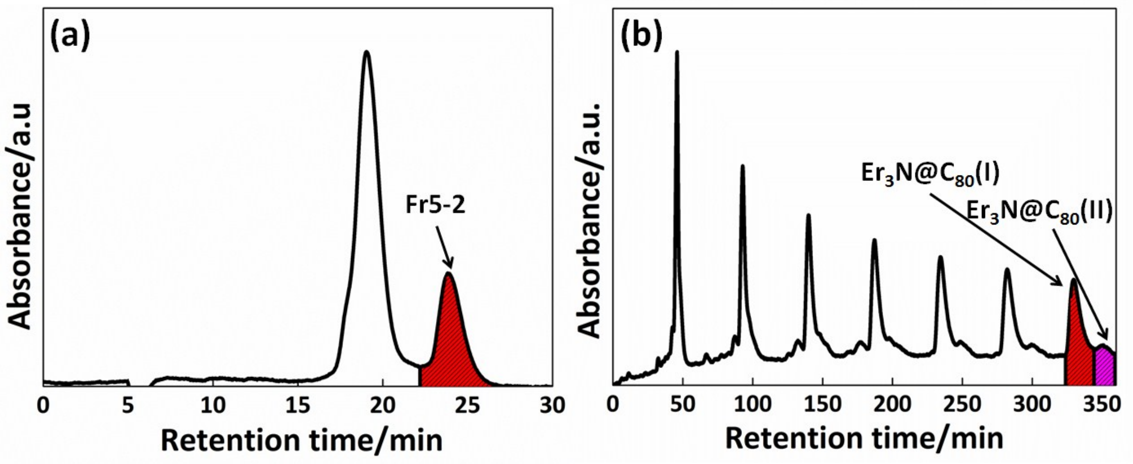

Fig. S2 Isolation schemes of $Er_3N@I_h(7)$-C_{80} and $Er_3N@D_{5h}(6)$-C_{80}. (a) HPLC chromatogram of Fr5 on a Buckyprep-M column. Conditions: 15 mL injection volume; 12 mL/min toluene flow. (b) Recycling HPLC chromatogram of Fr5-2 on a 5PBB column. Conditions: 10 mL injection volume; 10 mL/min chlorobenzene flow. (All of the detection wavelengths are 330 nm.)

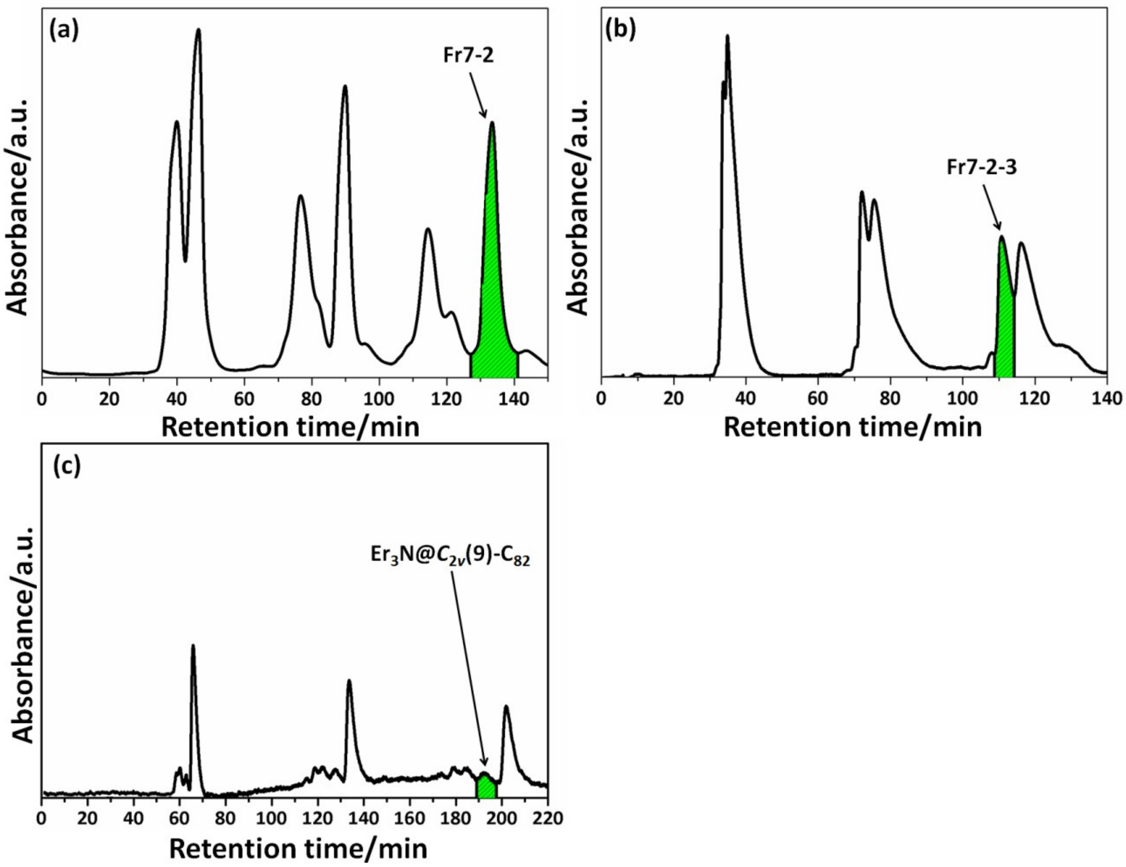

Fig. S3 Isolation schemes of $Er_3N@C_{2v}(9)-C_{82}$. (a) Recycling HPLC chromatogram of Fr7 on a Buckyprep-M column. Conditions: 30 mL injection volume; 8 mL/min toluene flow. (b) Recycling HPLC chromatogram of Fr7-2 on a 5PYE column. Conditions: 20 mL injection volume; 8 mL/min toluene flow. (c) Recycling HPLC chromatogram of Fr7-2-3 on a Buckyprep column. Conditions: 10 mL injection volume; 12 mL/min toluene flow. (All of the detection wavelengths are 330 nm.)

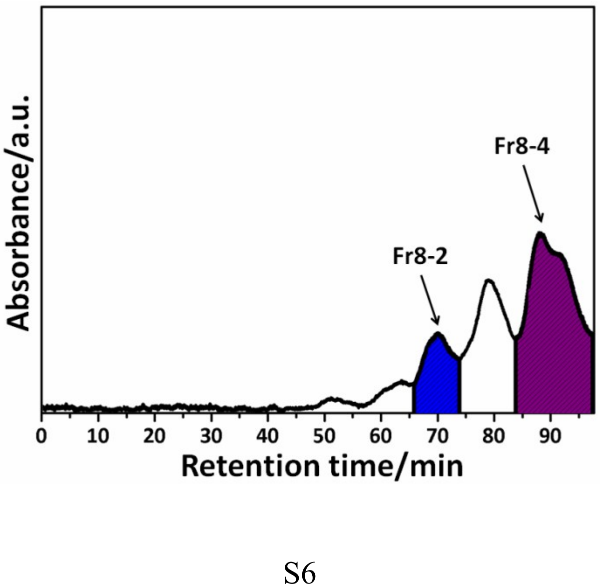

Fig. S4 Isolation schemes of Fr8 on a 5PBB column. Conditions: eluent: chlorobenzene, 10 mL/min flow rate; inject volume: 20 mL; 330 nm detecting wavelength.

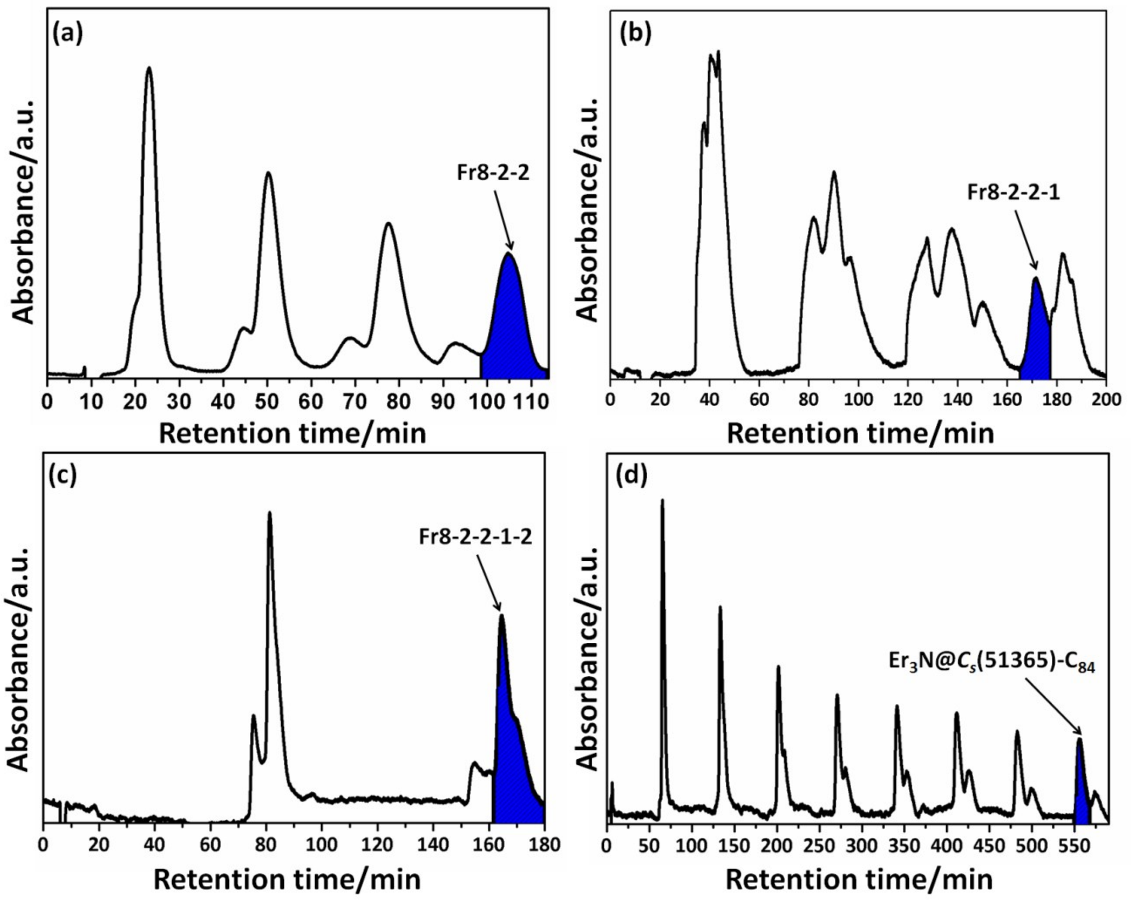

Fig. S5 Isolation schemes of $Er_3N@C_s(51365)-C_{84}$. (a) Recycling HPLC chromatogram of Fr8-2 on a Buckyprep-M column. Conditions: 20 mL injection volume; 7 mL/min chlorobenzene flow. (b) Recycling HPLC chromatogram of Fr8-2-2 on a Buckyprep column. Conditions: 15 mL injection volume; 5 mL/min chlorobenzene flow. (c) Recycling HPLC chromatogram of Fr8-2-2-1 on a Buckyprep column. Conditions: 15 mL injection volume; 10 mL/min toluene flow. (d) Recycling HPLC chromatogram of Fr8-2-2-1-2 on a Buckyprep column. Conditions: 15 mL injection volume; 12 mL/min toluene flow. (All of the detection wavelengths are 330 nm.)

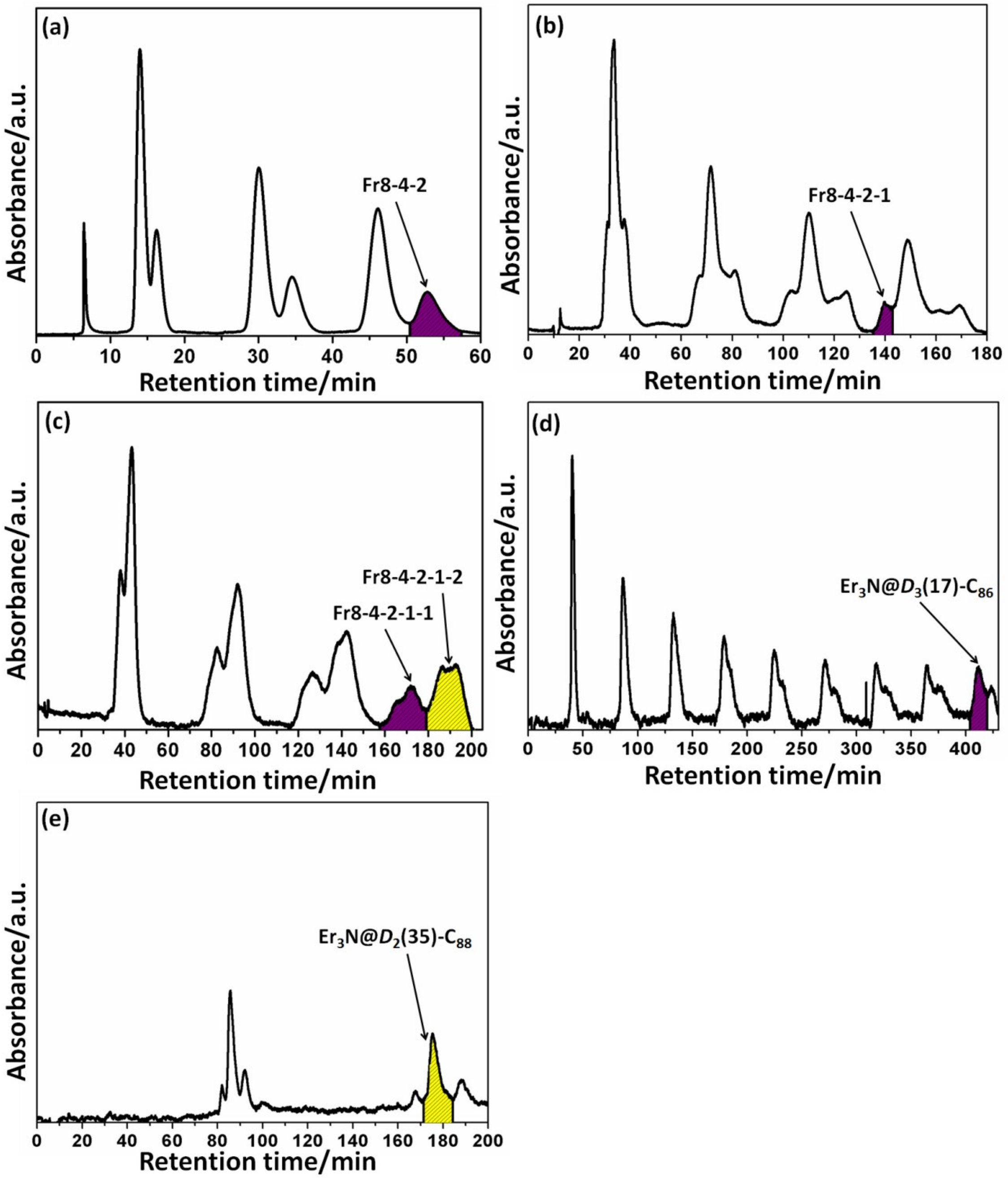

Fig. S6 Isolation schemes of $Er_3N@D_3(17)$-C_{86} and $Er_3N@D_2(35)$-C_{88}. (a) Recycling HPLC chromatogram of Fr8-4 on a Buckyprep-M column. Conditions: 10 mL injection volume; 10 mL/min chlorobenzene flow. (b) Recycling HPLC chromatogram of Fr8-4-2 on a Buckyprep column. Conditions: 10 mL injection volume; 6 mL/min chlorobenzene flow. (c) Recycling HPLC chromatogram of Fr8-4-2-1 on a 5PBB column. Conditions: 10 mL injection volume; 5 mL/min chlorobenzene flow. (d) Recycling HPLC chromatogram of Fr8-4-2-1-1 on a Buckyprep column. Conditions: 10 mL injection volume; 5 mL/min toluene flow. (e) Recycling HPLC chromatogram of Fr8-4-2-1-2 on a Buckyprep column. Conditions: 10 mL injection volume; 10 mL/min toluene flow. (All of the detection wavelengths are 330 nm.)

Table S1. The details of the vis-NIR absorptions of $Er_3N@C_{80\text{-}88}$ isomers.[a]

Compound	vis-NIR absorption bands (nm)	Onset (nm)	Optical bandgap (eV)[a]
$Er_3N@C_{80}$(I)	408, 562, 668, 701	748	1.66
$Er_3N@C_{80}$(II)	471	900	1.38
$Er_3N@C_{82}$	462, 681, 916	1223	1.01
$Er_3N@C_{84}$	471, 624	980	1.27
$Er_3N@C_{86}$	430, 644, 745	1026	1.21
$Er_3N@C_{88}$	471, 553, 729, 864, 1046	1295	0.96

[a] Optical bandgap (eV) ≈ 1240/onset (nm).

Table S2. Crystallographic data of $Er_3N@I_h(7)\text{-}C_{80}/Ni^{II}(OEP)$, $Er_3N@D_{5h}(6)\text{-}C_{80}/Ni^{II}(OEP)$, $Er_3N@C_{2v}(9)\text{-}C_{82}/Ni^{II}(OEP)$, $Er_3N@C_s(51365)\text{-}C_{84}/Ni^{II}(OEP)$, and $Er_3N@D_2(35)\text{-}C_{88}/1.5Ni^{II}(OEP)$.

Compound	$Er_3N@I_h(7)\text{-}C_{80}{\bullet}Ni^{II}(OEP){\bullet}2(C_6H_6)$	$Er_3N@D_{5h}(6)\text{-}C_{80}{\bullet}Ni^{II}(OEP){\bullet}2(C_6H_6)$	$Er_3N@C_{2v}(9)\text{-}C_{82}{\bullet}Ni^{II}(OEP){\bullet}2(C_6H_6)$	$Er_3N@C_s(51365)\text{-}C_{84}{\bullet}Ni^{II}(OEP){\bullet}1.81(C_6H_6){\bullet}0.19(CS_2)$	$Er_3N@D_2(35)\text{-}C_{88}{\bullet}1.5Ni^{II}(OEP)$
T, K	173(2)	173(2)	173(2)	100(2)	100(2)
λ, Å	0.71073	0.71073	0.71073	0.65250	0.82657
color/habit	black / block	black / block	black / block	black / block	black / block
crystal size, mm	0.32×0.30×0.22	0.30×0.26×0.16	0.22×0.20×0.10	0.15×0.10×0.10	0.20×0.18×0.10
Empirical formula	$C_{128}H_{56}Er_3N_5Ni$	$C_{128}H_{56}Er_3N_5Ni$	$C_{130}H_{56}Er_3N_5Ni$	$C_{131.05}H_{54.85}Er_3N_5Ni$	$C_{284}H_{132}Er_6N_{14}Ni_3$
fw	2224.25	2224.25	2248.30	2276.63	4919.33
crystal system	monoclinic	monoclinic	monoclinic	triclinic	monoclinic
space group	$C2/m$	$C2/m$	$C2/m$	$p\ \bar{\mathrm{I}}$	$C2/m$
a, Å	25.302(3)	25.309(5)	25.548(5)	14.5795(2)	24.8075(6)
b, Å	15.150(2)	15.149(5)	15.259(5)	14.9763(2)	18.1337(4)
c, Å	19.790(3)	19.789(5)	19.989(5)	19.7722(3)	22.2769(6)
α, deg	90.000	90.000	90.000	84.960(1)	90.000
β, deg	95.315(3)	95.267(5)	95.273(5)	89.147(1)	100.419(1)
γ, deg	90.000	90.000	90.000	62.3700	90.000
V, $Å^3$	7553.4(18)	7555(3)	7760(4)	3808.45(9)	9856.1(4)
Z	4	4	4	2	2
ρ, g/cm^3	1.956	1.955	1.924	1.985	1.657
μ, mm^{-1}	3.617	3.615	3.521	2.872	4.234
Data/restraints/parameters	8652/1410/1202	7260/2363/1184	9633/1973/1250	13720/2386/1336	9215/2563/1218
R1 [reflections with I>2σ(I)]	0.0385(7375)	0.0608(6498)	0.0917(6715)	0.0743(12976)	0.1507(7282)
wR2 (all data)	0.0971	0.1767	0.3079	0.1913	0.3711

Table S3. The fractional occupancies of the Er positions in $Er_3N@I_h(7)$-C_{80}, $Er_3N@D_{5h}(6)$-C_{80}, $Er_3N@C_{2v}(9)$-C_{82}, $Er_3N@C_s(51365)$-C_{84}, and $Er_3N@D_2(35)$-C_{88}.

EMFs	Fractional occupancy of the Er positions[a]													
$Er_3N@I_h(7)$-C_{80}	Er1/Er1A	Er2	Er3/Er3A	Er4/Er4A	Er5/Er5A	Er6	Er7/Er7A	Er8/Er8A	Er9	Er10/Er10A	Er11	Er12/Er12A	Er13/Er13A	Er14/Er14A
	0.24	0.23	0.22	0.22	0.21	0.21	0.14	0.07	0.06	0.03	0.03	0.02	0.02	0.02
	Er15/Er15A	Er16	Er17/Er17A	Er18/Er18A	Er19/Er19A									
	0.01	0.01	0.01	0.01	0.01									
$Er_3N@D_{5h}(6)$-C_{80}	Er1	Er2/Er2A	Er3/Er3A	Er4/Er4A	Er5	Er6	Er7/Er7A	Er8/Er8A	Er9/Er9A	Er10/Er10A	Er11/Er11A	Er12/Er12A	Er13/Er13A	Er14
	0.38	0.37	0.23	0.13	0.11	0.10	0.10	0.07	0.07	0.05	0.04	0.04	0.03	0.03
	Er15/Er15A	Er16	Er17/Er17A	Er18										
	0.02	0.02	0.02	0.02										
$Er_3N@C_{2v}(9)$-C_{82}	Er1/Er1A	Er2/Er2A	Er3/Er3A	Er4/Er4A	Er5/Er5A	Er6	Er7/Er7A	Er8/Er8A	Er9/Er9A	Er10	Er11/Er11A	Er12/Er12A	Er13/Er13A	Er14/Er14A
	0.22	0.18	0.18	0.12	0.11	0.10	0.08	0.07	0.06	0.05	0.05	0.05	0.05	0.04
	Er15/Er15A	Er16/Er16A	Er17	Er18/Er18A	Er19	Er20/Er20A	Er21/Er21A	Er22/Er22A						
	0.04	0.04	0.04	0.03	0.03	0.03	0.02	0.02						
$Er_3N@C_s(51365)$-C_{84}	Er1	Er2	Er3	Er4	Er5	Er6	Er7	Er8	Er9	Er10	Er11	Er12	Er13	Er14
	0.22	0.10	0.24	0.70	0.20	0.03	0.01	0.24	0.02	0.04	0.05	0.07	0.02	0.02
	Er15	Er16	Er17	Er18	Er19	Er20	Er21	Er22	Er23	Er24	Er25	Er26	Er27	Er28
	0.02	0.20	0.09	0.02	0.09	0.03	0.13	0.02	0.10	0.10	0.03	0.16	0.03	0.02
$Er_3N@D_2(35)$-C_{88}	Er1/Er1A	Er2	Er3/Er3A	Er4/Er4A	Er5/Er5A	Er6/Er6A	Er7/Er7A	Er8	Er9/Er9A	Er10	Er11/Er11A	Er12	Er13	Er14/Er14A
	0.11	0.17	0.04	0.15	0.11	0.10	0.13	0.19	0.10	0.12	0.07	0.07	0.08	0.09
	Er15/Er15A	Er16/Er16A	Er17	Er18/Er18A	Er19	Er20	Er21							
	0.04	0.09	0.05	0.05	0.07	0.06	0.03							

[a] The atom with a suffix ‘A’ is generated by crystallographic operation.

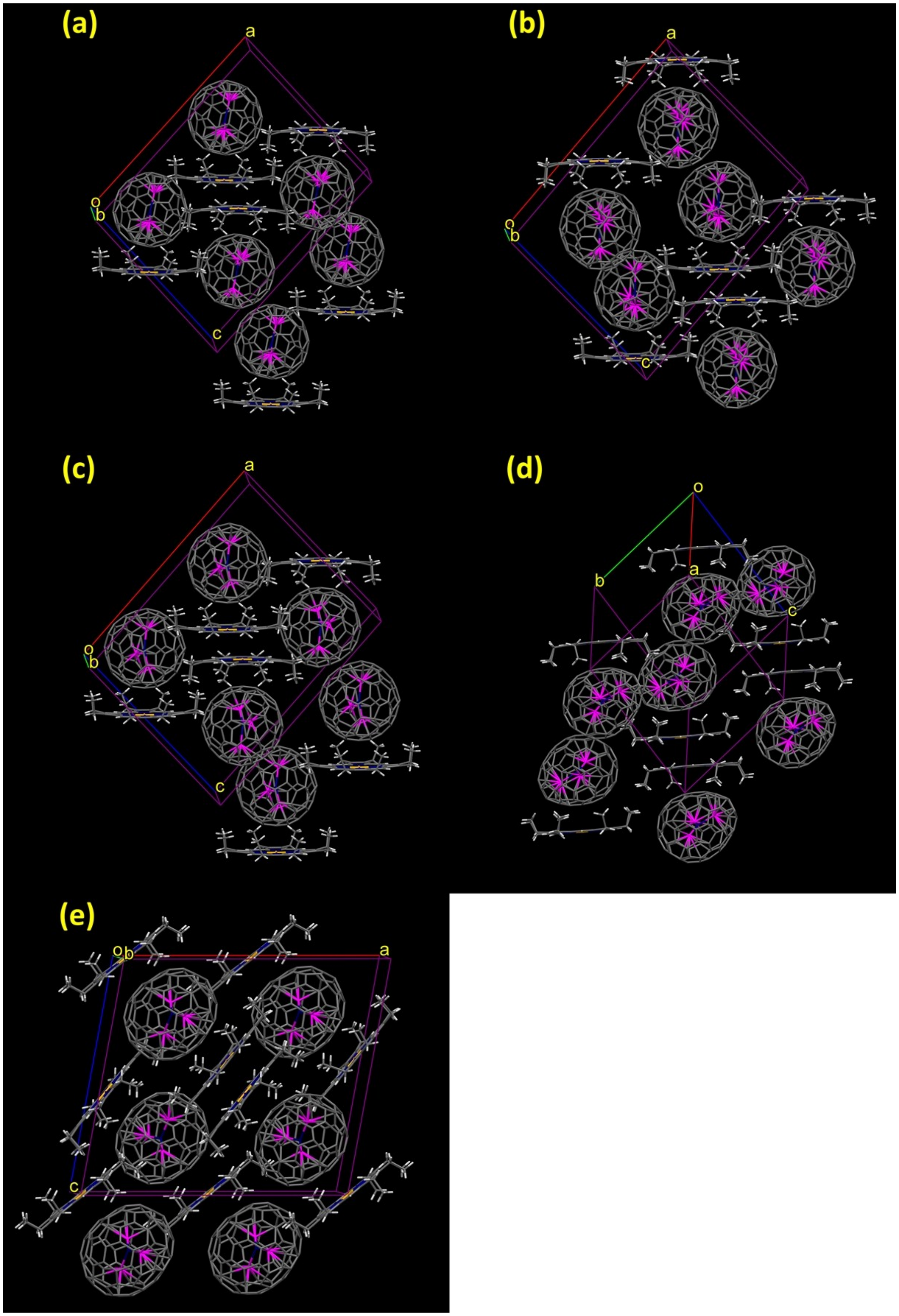

Fig. S7 Packing structures of (a) $Er_3N@I_h(7)\text{-}C_{80}\cdot Ni^{II}(OEP)$, (b) $Er_3N@D_{5h}(6)\text{-}C_{80}\cdot Ni^{II}(OEP)$, (c) $Er_3N@C_{2v}(9)\text{-}C_{82}\cdot Ni^{II}(OEP)$, (d) $Er_3N@C_s(51365)\text{-}C_{84}\cdot Ni^{II}(OEP)$, and (e) $Er_3N@D_2(35)\text{-}C_{88}\cdot 1.5Ni^{II}(OEP)$ with minor disordered components and solvents omitted for clarity.

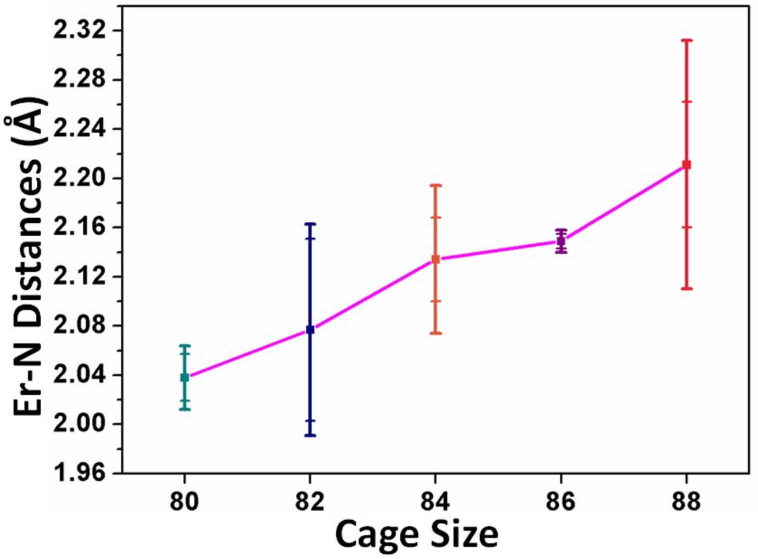

Fig. S8 The Er-N distances of the major Er_3N site as a function of the cage size. (Values for $Er_3N@C_{86}$ are obtained in theory.)

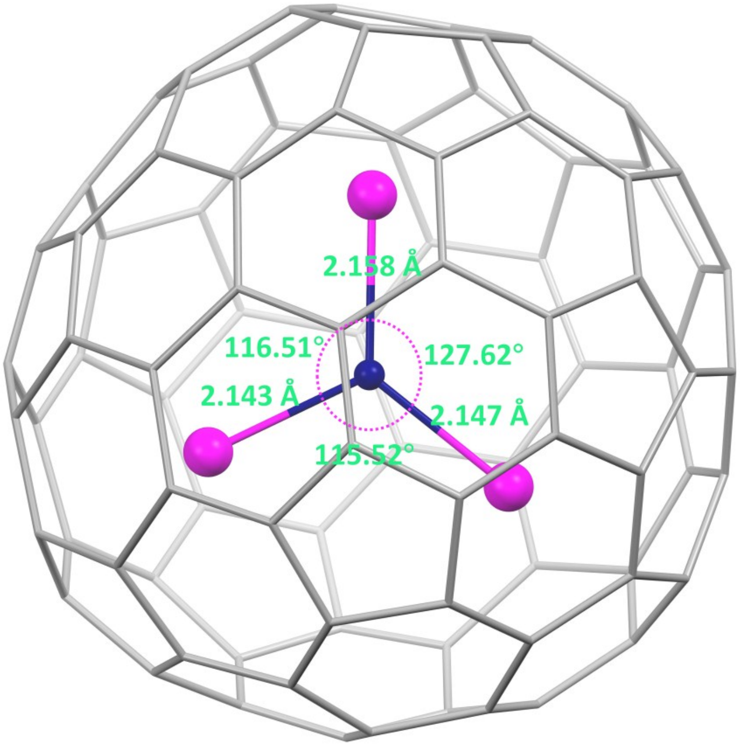

Fig. S9 Optimized molecular structure of $Er_3N@D_3(17)\text{-}C_{86}$.

Table S4. Main molecular orbital energy levels (eV) of $Er_3N@I_h(7)$-C_{80}, $Er_3N@D_{5h}(6)$-C_{80}, $Er_3N@C_{2v}(9)$-C_{82}, $Er_3N@C_s(51365)$-C_{84}, $Er_3N@D_3(17)$-C_{86}, and $Er_3N@D_2(35)$-C_{88} at the UB3LYP/3-21G~SDD~ECP28MWB_SEG level of theory.

Compound	LUMO+2		LUMO+1		LUMO		HOMO		HOMO-1		HOMO-2	
	α	β	α	β	α	β	α	β	α	β	α	β
$Er_3N@C_{80}$(I)	-2.76	-3.16	-2.91	-3.23	-3.17	-3.31	-5.90	-5.93	-6.03	-6.02	-6.04	-6.07
$Er_3N@C_{80}$(II)	-2.98	-3.13	-3.02	-3.21	-3.18	-3.26	-5.63	-5.64	-5.70	-5.75	-6.00	-6.01
$Er_3N@C_{82}$	-2.92	-3.37	-2.93	-3.44	-3.50	-3.65	-5.25	-5.32	-5.57	-5.63	-6.21	-6.22
$Er_3N@C_{84}$	-2.83	-3.48	-3.04	-3.56	-3.24	-3.58	-5.52	-5.53	-5.75	-5.78	-6.16	-6.18
$Er_3N@C_{86}$	-3.00	-3.50	-3.12	-3.51	-3.18	-3.53	-5.55	-5.59	-5.62	-5.65	-5.78	-5.81
$Er_3N@C_{88}$	-2.94	-3.65	-3.30	-3.68	-3.38	-3.72	-5.24	-5.30	-5.77	-5.79	-6.17	-6.19

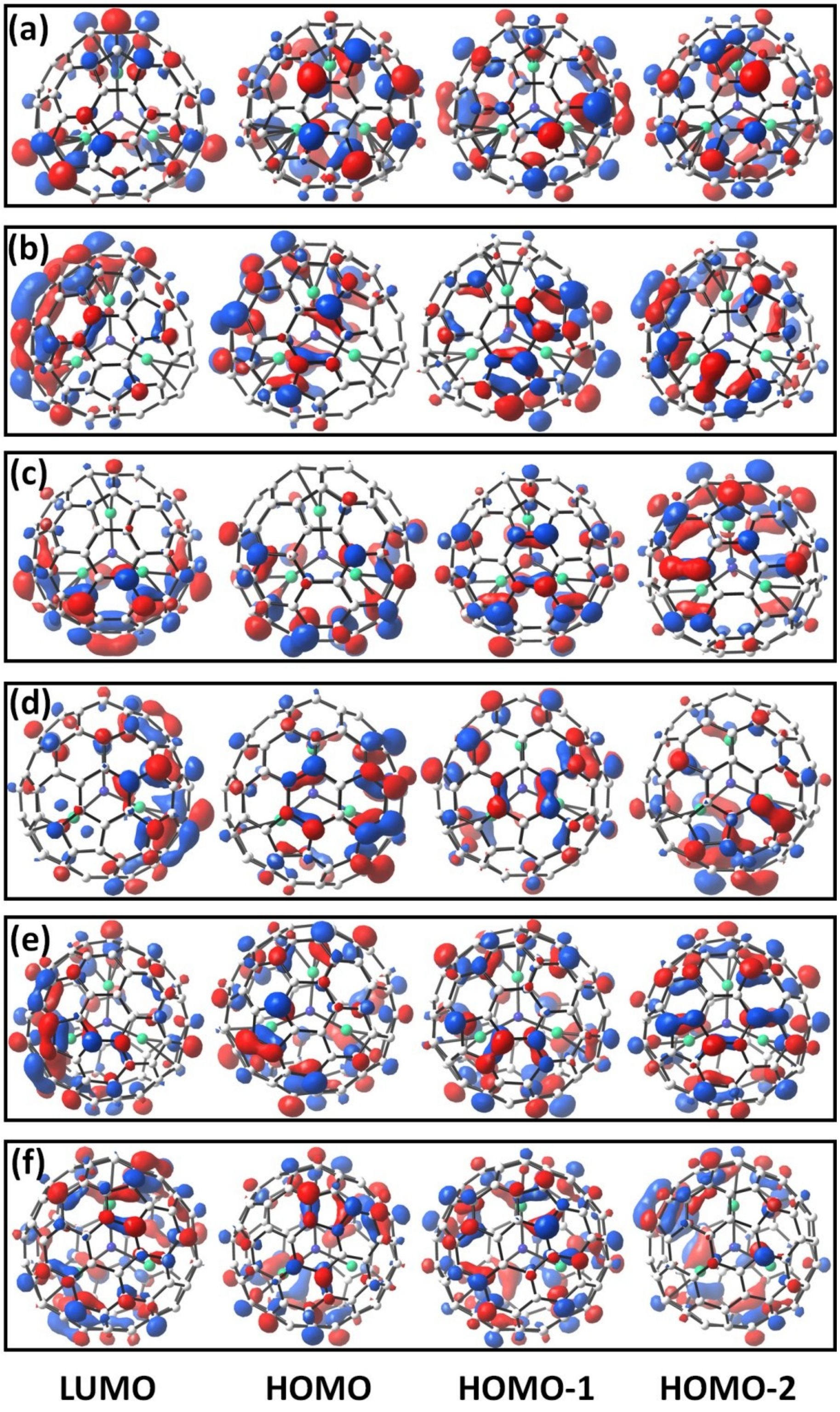

Fig. S10 Main molecular orbitals of (a) $Er_3N@I_h(7)-C_{80}$, (b) $Er_3N@D_{5h}(6)-C_{80}$, (c) $Er_3N@C_{2v}(9)-C_{82}$, (d) $Er_3N@C_s(51365)-C_{84}$, (e) $Er_3N@D_3(17)-C_{86}$, and (f) $Er_3N@D_2(35)-C_{88}$ at the UB3LYP/3-21G~SDD~ECP28MWB_SEG level of theory (Isovalue = 0.03).

References:

1. Q.-S. Wang, K.-H. Zhang, Y. Cui, Z.-J. Wang, Q.-Y. Pan, K. Liu, B. Sun, H. Zhou, M.-J. Li, Q. Xu, C.-Y. Xu, F. Yu and J.-H. He, *Nuclear Science and Techniques*, 2018, **29**, 68.
2. G. M. Sheldrick, *Acta Crystallographica a-Foundation and Advances*, 2015, **71**, 3-8.
3. A. D. Becke, *Physical Review A*, 1988, **38**, 3098-3100.
4. A. D. Becke, *The Journal of Chemical Physics*, 1993, **98**, 5648-5652.
5. C. Lee, W. Yang and R. G. Parr, *Physical Review B*, 1988, **37**, 785-789.
6. D. Andrae, U. Häußermann, M. Dolg, H. Stoll and H. Preuß, *Theoretica chimica acta*, 1990, **77**, 123-141.
7. M. Dolg, H. Stoll and H. Preuss, *The Journal of Chemical Physics*, 1989, **90**, 1730-1734.
8. M. J. Frisch, G. W. Trucks, H. B. Schlegel, G. E. Scuseria, M. A. Robb, J. R. Cheeseman, G. Scalmani, V. Barone, B. Mennucci, G. A. Petersson, H. Nakatsuji, M. Caricato, X. Li, H. P. Hratchian, A. F. Izmaylov, J. Bloino, G. Zheng, J. L. Sonnenberg, M. Hada, M. Ehara, K. Toyota, R. Fukuda, J. Hasegawa, M. Ishida, T. Nakajima, Y. Honda, O. Kitao, H. Nakai, T. Vreven, J. A. Montgomery, Jr., J. E. Peralta, F. Ogliaro, M. Bearpark, J. J. Heyd, E. Brothers, K. N. Kudin, V. N. Staroverov, R. Kobayashi, J. Normand, K. Raghavachari, A. Rendell, J. C. Burant, S. S. Iyengar, J. Tomasi, M. Cossi, N. Rega, J. M. Millam, M. Klene, J. E. Knox, J. B. Cross, V. Bakken, C. Adamo, J. Jaramillo, R. Gomperts, R. E. Stratmann, O. Yazyev, A. J. Austin, R. Cammi, C. Pomelli, J. W. Ochterski, R. L. Martin, K. Morokuma, V. G. Zakrzewski, G. A. Voth, P. Salvador, J. J. Dannenberg, S. Dapprich, A. D. Daniels, Ö. Farkas, J. B. Foresman, J. V. Ortiz, J. Cioslowski and D. J. Fox, *Gaussian 09, Revision E.01,* Gaussian, Inc., Wallingford CT, 2013.